Applications in Energy and Combustion Science 22 (2025) 100338

Contents lists available at ScienceDirect

Applications in Energy and Combustion Science

journal homepage: www.sciencedirect.com/journal/applications-in-energy-and-combustion-science

Experimental analysis of swirl number and nozzle design for scale-up of partially cracked ammonia flames

Jordan Davies [a,*], Daisuke Sato [a,b], Syed Mashruk [a], Agustin Valera-Medina [a]

[a] College of Physical Sciences and Engineering, Cardiff University, Wales CF24 3AA. UK
[b] Department of Mechanical Engineering and Science, Kyoto University, Kyoto daigaku-Katsura, Nishikyo-ku, Kyoto 615-8540, Japan

ARTICLE INFO

Keywords:
Cracked ammonia
Swirl burner
Scale-up
Emissions

ABSTRACT

Due to its ease of storage and existing global distribution network, interest in the use of renewably produced ammonia for decarbonising energy systems is growing. Partially cracking ammonia can overcome the flame stability challenges of this fuel, but demonstrations of high-power ammonia-based swirl flames with acceptable emissions have yet to be realised. Therefore, the present study examines the effects of varying swirl number and nozzle design on the static stability and emissions from 20 % (vol.) cracked ammonia swirl flames for a wide range of equivalence ratios ($0.3 < \Phi < 2.2$) and thermal powers of 5, 10 and 15 kW. Additionally, a reference case of 100 kW thermal power at stoichiometric conditions was tested. Stable flames were shown across a broad range of equivalence ratios, swirl numbers and nozzle geometries although flame morphologies varied greatly. Of note was a geometric swirl number of 1.75 paired with a long nozzle, which enabled the transition to a flat, Coanda jet flow flame at equivalence ratios of 0.6 and 0.7. For a geometric swirl number of 1.45, shortening the nozzle resulted in significantly shorter, wider V-shape flames with greatly improved rich blowoff limits. This was found to be a desirable characteristic for reaching high thermal power with a constant nozzle throat diameter – i.e. dump plane velocity – as a widened flame brush prevents jet-like flames, which are susceptible to pinching off. This can also be achieved by increasing the swirl number, although to a lesser extent. However, with a widened flame brush, careful consideration must be given to confinement diameter to avoid flame impingement which has potential to increase local heat loss and hence reduce combustion efficiency, resulting in an increase in unburned NH_3 emissions. With the same geometric swirl number of 1.45, the shorter nozzle configuration resulted in higher NO emissions, potentially due to the shorter nozzle forming shorter, wider flames, meaning there was less residence time for NH_2 to consume NO in the flame zone. This difference was less noticeable at rich conditions, with all configurations reaching negligible NO emissions by $\Phi = 1.15$

1. Introduction

Interest in the use of partially cracked ammonia for the decarbonisation of energy is growing. This is due to ammonia's ease of transportation and existing global infrastructure [1–3]. The main challenges relating to combustion of pure ammonia – low flame stability and emissions of NOx – can be addressed by mixing ammonia with a relatively small amount of hydrogen [4,5]. This can be achieved by partially cracking the ammonia with integrated thermo-catalytic systems [6], resulting in a final fuel blend of ammonia, hydrogen and nitrogen.

The earliest studies on ammonia combustion in gas turbine swirl burners were published in the 1960s [7], with main findings including narrow stability limits and the requirement of air velocity being half of what they were for hydrocarbon fuels. Few publications can be found between then and the mid-2010s.

However, swirl stabilised combustion of ammonia/hydrogen-based blends has seen renewed research in the last decade, mainly examining emissions or flame stability with fixed swirl numbers. Many research groups have presented effective flame stabilisation with this method at relatively low thermal power, in the order of tens of kW. In 2015, Cardiff University tested blends of NH_3/CH_4 as high as 80/20 (vol. %) and NH_3/H_2 of 50/50 (vol. %) in a generic tangential swirl burner designed for natural gas with a swirl number of 1.05 [8]. For the NH_3/H_2 case of 33 kW thermal power, narrow stability limits between equivalence ratios (Φ) of just 0.425 and 0.577 were possible, with flashback preventing any further increases in Φ. This suggested that generic

* Corresponding author.
E-mail address: daviesj129@cardiff.ac.uk (J. Davies).

https://doi.org/10.1016/j.jaecs.2025.100338
Received 14 March 2025; Received in revised form 19 May 2025; Accepted 20 May 2025
Available online 20 May 2025

swirlers from natural gas combustors may not necessarily be suited to NH_3/H_2 blends.

In 2017, Kurata et al. demonstrated power generation from a converted kerosene MGT operating on pure NH_3 [9]. The MGT featured a non-premixed axial swirl burner with swirl number of 0.88. Good flame stability was found, but it was noted that elevated inlet temperatures would widen stability limits. Later, using a similar combustor, Okafor et al. found that compared to atmospheric conditions, increasing the pressure to 0.2 MPa reduced NO emissions without any apparent penalty in flame stability nor unburned NH_3 emissions [10].

An early study from Tohoku University compared two different axial swirlers with swirl numbers of 0.736 and 1.270 in the combustion of pure NH_3 at a thermal power of 13.2 kW [11]. Although narrower than those of CH_4, the stability limits of NH_3 were found to be broad, roughly $0.65 < \Phi < 1.3$ for an inlet velocity between 2 and 8 m/s for the high swirl case, and slightly wider for the low swirl case. The authors suggested the lower swirl number presented wider stability limits due to a higher characteristic length of recirculation aiding the slow combustion rate. This study also presented slightly rich conditions of $\Phi = 1.05$ as optimal, with relatively low emissions of both NO and NH_3.

In 2019, a marked increase in research of NH_3 combustion in swirl burners can be seen. Continued studies from Cardiff University found a 70/30 NH_3/H_2 blend (vol. %) provided stable flame at slightly rich conditions using a tangential swirl number of 0.8 at a thermal power of 39.3 kW [12]. The same swirl burner and fuel blend was also found to provide stable combustion at elevated conditions of up to 0.184 MPa and with humidification and secondary air injection [13]. It was noted that the limiting factor in increasing pressure further was fuel supply of gaseous ammonia, not flame stability.

Initial studies at KAUST on NH_3/H_2 blends using a swirl burner with swirl number of 1.0 and thermal power of <10 kW [14] found narrow stability limits bounded by lean blowoff and flashback when the ammonia fuel fraction was <60 % (vol.). Above this, stability limits widened significantly and the 70/30 (vol. %) NH_3/H_2 was bounded by lean blowoff at $\Phi = 0.3$, but instead of the upper boundary being flashback, it was found to be rich blowoff, at $\Phi = 1.4$. Increasing NH_3 fraction further resulted in a slight narrowing of stability limits – although still significantly wider than below 60 % NH_3, with upper limits still bounded by rich blowoff rather than flashback. Following research with the same swirl burner increased thermal power to 32.5 kW and pressure to 5 bar [15]. Here, it was found that pressurisation increases stability limits of pure NH_3 flames. For NH_3/H_2 blends, both lean blowout and flashback limits were slightly reduced with pressure. Additionally, the NH_3 fuel fraction threshold at which the upper limit of stability transitioned from flashback to rich blowoff was increased. Another study from Wang et al. of KAUST utilising an adjustable axial swirl burner examined the effects of varying swirl number between 0.6 and 1.0 on emissions from NH_3/CH_4 flames [16]. Stable flames were found for both swirlers in the range $0.55 < \Phi < 0.95$. Additionally, this study showed a significant difference in both flame structure and NO emissions, with the higher swirl flame presenting lower NO emissions above $\Phi = 0.75$. This was suggested to be due to the higher swirl flame having higher heat loss to the nozzle, inhibiting the formation of OH radicals in this region.

A recent study from Chen et al. of USTC [17] examined OH* chemiluminescence from a range of ammonia blended flames with a swirl number of 0.778. They found that partially cracked ammonia flames were narrower and longer than equivalent NH_3/H_2 flames and had a higher peak value of OH*, indicating the stretching effect was stronger. This has potential to affect blowoff limits in partially cracked ammonia flames, warranting further study compared to classical NH_3/H_2 blends.

It is clear to see that most research groups have been operating NH_3 based flames with relatively low swirl numbers between 0.6 and 1.05. Despite this rich literature of ammonia swirl flames, it remains that few studies have drawn comparisons between swirl number and flame performance, either in terms of emissions or stability limits, particularly for NH_3/H_2 flames. Therefore, the present study seeks to further the deployment of swirl burners operating on partially cracked ammonia blends in an industrial setting by investigating how swirl number and nozzle design affects flame stability and emissions. A particular focus is given to how these swirlers perform with an increase in thermal power towards industrially applicable levels.

2. Experimental methodology

2.1. Swirl burner

In this study, the optically accessible premixed atmospheric swirl burner shown in Fig. 1 was used. Air and fuel entered a premixing chamber via Bronkhorst thermal mass flow controllers with accuracy of ± 0.5 % of reading between 15 % and 95 % of full scale. A constant fuel blend representing 20 % cracked ammonia (66.7/25/8.3 (vol. %) $NH_3/H_2/N_2$) for equivalence ratios $0.3 < \Phi < 2.2$ and three net thermal powers; 5, 10 and 15 kW was used. Additionally, a reference case was preliminarily examined where the same swirl burner was placed inside a significantly larger confinement representative of a 1MW steam boiler. Here, the net thermal power was increased to 100 kW and stoichiometric conditions were examined for the same 20 % cracked NH_3 fuel blend. 20 % cracked ammonia includes the nitrogen produced during the cracking process in the required 3:1 hydrogen/nitrogen ratio while maintaining the NH_3/H_2 ratio near to 70/30 (vol. %). This fuel blend was used due to it having previously been identified as an optimal NH_3/H_2 ratio [13], balancing improved flame stability from hydrogen addition [4] with penalties in exhaust gas emission [18]. While this fuel blend generally has a lower laminar burning velocity than pure methane flames, the differences are smaller at lean and rich conditions [19]. Additionally, 20 % cracked ammonia flames have been found to have the highest ratio of turbulent flame speed to laminar flame speed of partially cracked blends [20], indicating they may have higher blowoff resistance than suggested solely by their laminar flame speed. Furthermore, an 18 % cracked ammonia flame (very similar to the fuel blend in this study) has been shown to have higher lean blowoff resistance than pure methane flames due to higher positive flame curvatures and lower strain rates resulting from a Lewis number below unity [21,22].

A range of tangential swirlers and nozzles were investigated, described in Table 1. The geometric swirl number was defined as shown in Eq. (1), reproduced from [23].

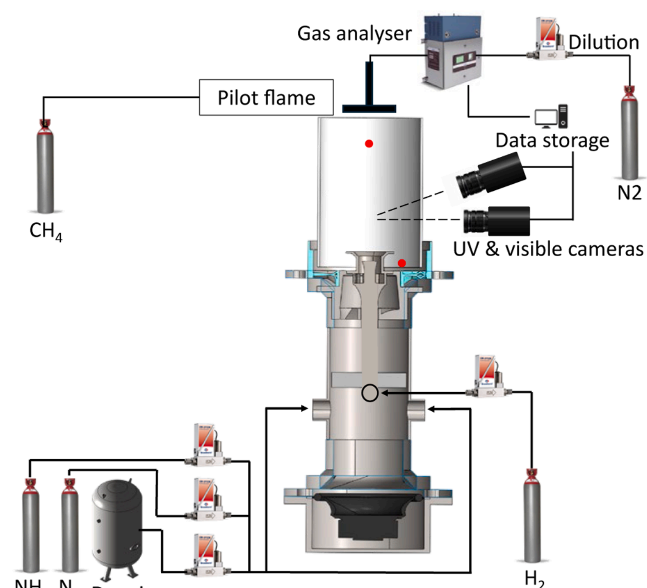

Fig. 1. Simplified schematic of experimental setup.

Table 1
Description of swirl number and nozzle geometries.

S_g	Nozzle	Thermal Power (kW)	Φ Tested
1.0	Short	5, 10, 15	$0.3 < \Phi < 2.2$
1.45	Short	5, 10, 15, 100	$0.3 < \Phi < 2.2$
1.45	Long	5, 10, 15, 100	$0.3 < \Phi < 2.2$
1.75	Long	5, 10, 15	$0.3 < \Phi < 2.2$

$$S_g = \frac{\pi R R_{eff}}{A_t} \tag{1}$$

Where R was the exit radius, R_{eff} was the radial distance between each tangential channel axis and the injector axis, and A_t was the cross-sectional area of the tangential channels. The different geometric swirl numbers were achieved by varying A_t.

As shown in Fig. 2, the nozzle inner diameter (D) and bluff body outer diameter (0.7 D) were constant for all cases. The confinement consisted of a quartz tube of inner diameter 5D and length 9.5D, resulting in an expansion ratio from the dump plane area to confinement area of 50.1. The nozzle geometry was varied by changing the axial length of the nozzle. In Fig. 2, the dashed red line shows the approximate position of the original dump plane with a long nozzle, and the black solid line shows the modified dump plane position with a shorter nozzle. The long nozzle had a greater distance from the dump plane to nozzle expansion section than the short nozzle, but the dump plane cross-sectional area was kept constant for all conditions and cases.

2.2. Flame imaging

A Nikon Z7ii mirrorless digital camera was used to capture direct line of sight images of the flame from a distance of approximately 500 mm. Unless otherwise stated, the camera's aperture was maintained at F/4 with an exposure time of 1/3 s and an ISO of 64 for all photographs to enable comparisons of flame morphology and intensity.

Chemiluminescence images were captured by LaVision cameras comprising Sony ICX285AL sensors and Hamamatsu HB1058 intensifiers. Edmund optics bandpass filters all with 10 nm FWHM centred at 310 nm, 337 nm and 632 nm were used to capture OH* (309 nm; A2Σ + -X2Π system), NH* (336 nm; A3Π-X2Σ system) and NH_2* (630 nm; single peak of NH_2 α band), respectively. These cameras were triggered simultaneously for a period of 20 s at a sampling rate of 10 Hz. Following the subtraction of the background images and a 3 × 3 median pixel filter, the images were averaged and processed with an Abel Deconvolution script [24]. Abel transformed images were either normalised to their own maximum to compare flame morphology or to group maximums to compare radical intensities across different swirlers and nozzle setups.

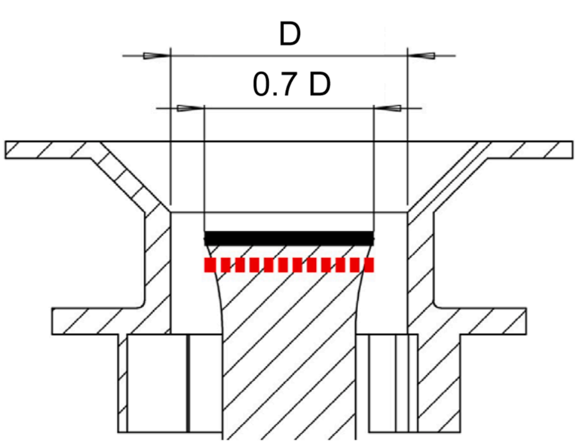

Fig. 2. Diagram of swirler and nozzle (black and red dashed lines show position of dump plane relative to nozzle walls with a short and long nozzle, respectively).

2.3. Exhaust gas measurements

Exhaust gas samples were captured via a cross-shaped sampling probe spanning the full diameter of the quartz tube confinement outlet. To prevent condensation, the sample gas was carried along a heated line to an Emerson CT5100 quantum cascade laser gas analyser. Measurements of NO, NO_2, N_2O, NH_3, O_2 and H_2O were made at a temperature of 463 K and rate of 1 Hz (±1 % repeatability, 0.999 linearity). At each test condition and following the stabilisation of inlet flowrates, temperatures and emissions, 120 samples were recorded over a period of two minutes. When raw readings were above the analyser's upper detection limit (~2200 ppm for NO and ~1300 ppm for NH_3), N_2 was used to dilute the sample back into range ((±10 % repeatability). Samples were captured wet and normalised to dry, 15 % O_2 following equation 10 in [25]. As this study focuses solely on a single blend of partially cracked ammonia with relatively constant concentrations of H_2O present in the exhaust gas, there was no need to use other emissions normalisation methodologies which account for high levels of H_2O dilution arising from hydrogen-based fuels in comparison to hydrocarbon fuels.

3. Results and discussion

3.1. Flame morphology and stability

Fig. 3 shows direct line of sight photographs captured for each of the four swirlers for a range of equivalence ratios at a constant net thermal power of 10 kW. In general, flame length increased with equivalence ratio at rich conditions regardless of swirl number. For $0.7 < \Phi < 1.0$, flame length was relatively consistent for all cases, apart from for the Sg = 1.75 long nozzle case which presented as a nearly flat flame at the leanest equivalence ratios. Flame luminosity – largely from NH_2* – increased with equivalence ratio and was particularly low at $\Phi = 0.6$ for all swirlers, suggesting reduced combustion efficiency here.

With a constant swirl number of $S_g = 1.45$, the length of the nozzles can be seen to have a significant impact on flame morphology. The $S_g = 1.45$ long nozzle case presented a markedly longer flame than the $S_g = 1.45$ short nozzle case with a higher flame base angle at all equivalence ratios. It is suggested that a longer nozzle downstream of the bluff body acts as a guide channel, restricting the flow from expanding and thus hindering the formation of the external recirculation zone (ERZ) until further downstream. Similarly, this guide channel preventing the flow from expanding radially could result in the flow returning to the central axis shortly downstream of the bluff body, resulting in the central recirculation zone (CRZ) being compressed axially. The long nozzle case then may not properly expand radially until reaching a vortex breakdown bubble further downstream. Alternatively, the short nozzle case had less of a radial obstruction downstream of the bluff body, enabling the flow to open radially earlier, forming a stronger ERZ and CRZ. At rich equivalence ratios, this effect was even clearer, with the long nozzle flame transitioning into a near jet-like flame shape with a potential reduction of the central recirculation zone (CRZ) strength.

Comparing the two short nozzle cases, increasing swirl number also reduced flame length and flame base angle, suggesting that nozzle geometry can be equally as important as swirl number in determining flame morphology. In comparing the two long nozzle cases, the same findings of increasing swirl number were present and more noticeable. This could suggest that the nozzle design may be the dominant design factor influencing flame morphology. The $S_g = 1.75$ long nozzle case did not present the same flame transition to near jet-like behaviour at rich conditions as the $S_g = 1.45$ long nozzle case. Additionally, there was a transition at lean conditions. At $\Phi \leq 0.7$, the $S_g = 1.75$ long nozzle case presented an almost flat flame with an exceptionally short flame length and near zero flame base angle. At higher equivalence ratios, a more conventional V-shaped swirl flame was found. This flat flame has been

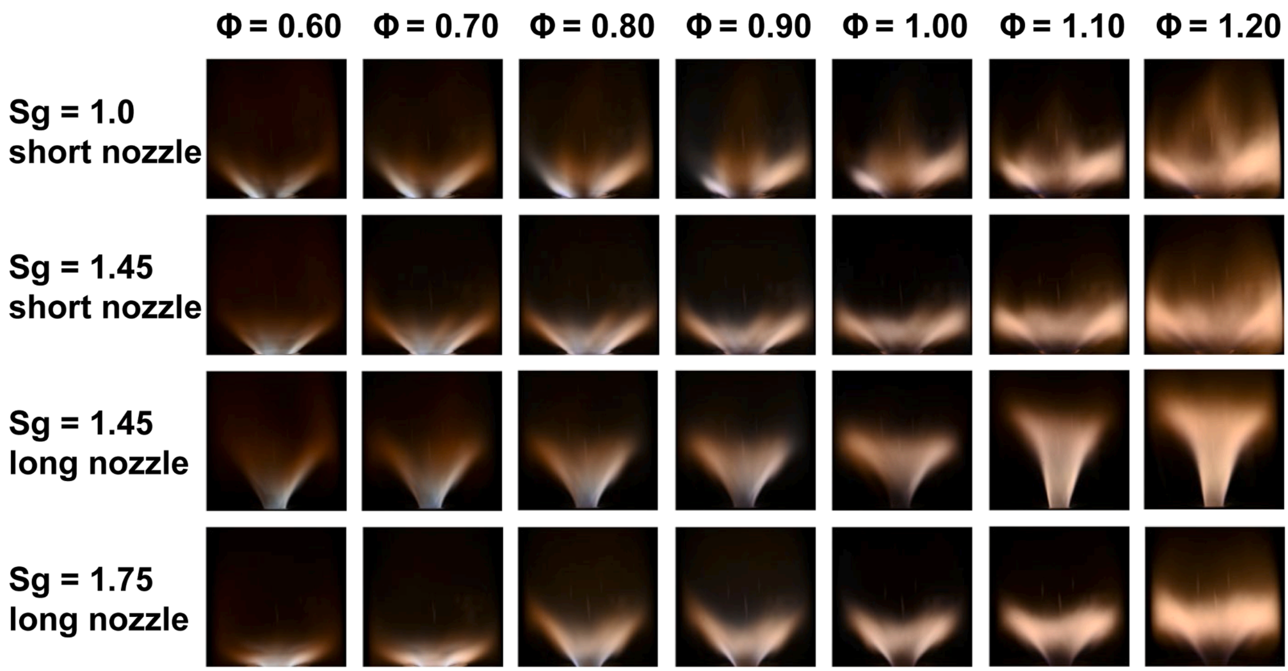

Fig. 3. Flame images for each of the swirlers examined at a range of equivalence ratios. Thermal power 10 kW. Image area 160 × 160 mm.

previously reported in the literature, where a swirling flow can transition from an open jet flow with high swirl to a Coanda jet flow (CJF) [26]. This transition is associated with high swirl numbers causing vortex breakdown to move further upstream into the nozzle until a negative axial velocity is found within the nozzle itself, forcing a transition to a CJF [27]. This would suggest a longer nozzle like in the Sg = 1.75 long nozzle case would be more susceptible to forming a CJF as the vortex breakdown would not have to travel so far axially before triggering the transition to CJF. Furthermore, the transition to CJF has been found to be more likely to occur with higher swirl numbers, and a higher swirl number is required to form a CJF when Reynolds number increases [28]. As the thermal power is constant in this study, the Reynolds number increases with a reduction in equivalence ratio. This could explain why only the $S_g = 1.75$ long nozzle case formed a Coanda jet flow flame. It is the only case which has both a long enough nozzle and high enough swirl number to form a CJF at the relatively high Reynolds number found at $\Phi = 0.7$ as the vortex breakdown becomes dominant with reduced heat release rates at lean conditions. This CJF flame was observed for the $S_g = 1.75$ long nozzle case at 5 kW thermal power, but not at 15 kW. This could be because it was not experimentally possible to reach lean enough conditions for it to form at 15 kW, or because the Reynolds number was too high at 15 kW for a CJF to form at this swirl number.

It can also be seen that both the long nozzle cases had a narrow flame root, anchored to the bluff body. In comparison the short nozzle cases both anchored on the nozzle outlet instead, resulting in a lower flame base angle and wider, more open flame. It is posited that this is a desirable characteristic for maintaining static flame stability at high

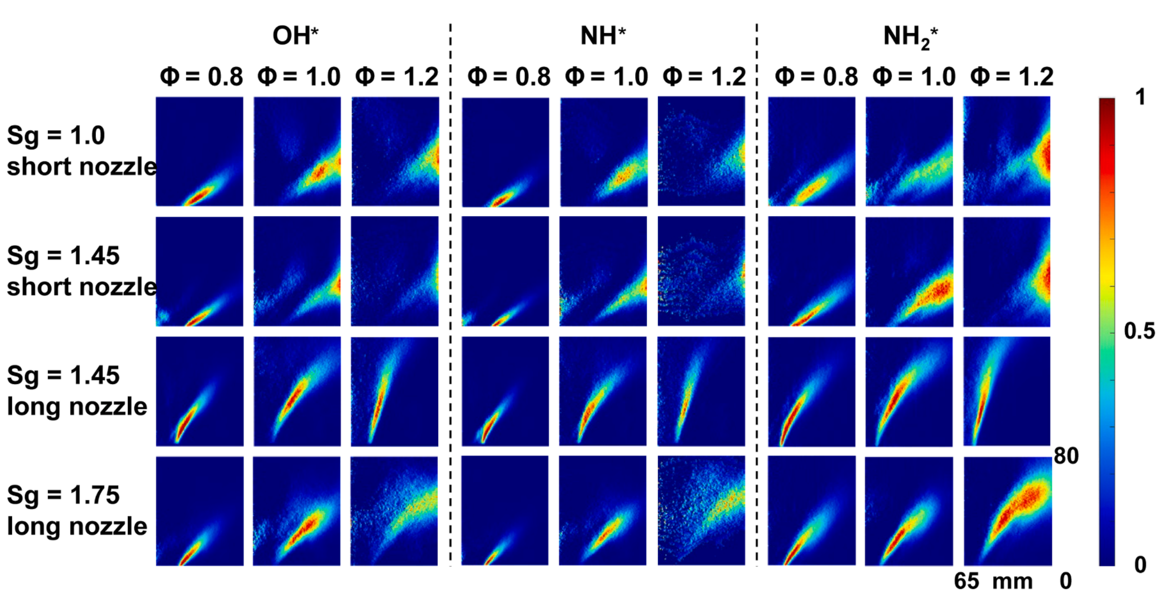

Fig. 4. Right half of Abel transformed chemiluminescence images (OH*, NH* and NH_2*) for each of the four cases at lean, stoichiometric and rich conditions and 10 kW. Colourmap of images normalised to each image's maximum intensity.

thermal powers with high dump plane velocities.

These same conditions were examined in more detail by utilising chemiluminescence imaging of OH*, NH* and NH_2*, shown in Fig. 4. As expected, similar findings in terms of flame length, base angle and anchoring location as from the direct line of sight photos in Fig. 3 can be seen again. However, some new information can still be gained. For example, for the short nozzle cases – at stoichiometric and slightly rich conditions, the radical intensity of OH*, NH* and NH_2* was reduced in the region near the nozzle. This is clearest to see for NH_2*, with the highest intensity region being relatively far from the nozzle outlet. In comparison, both long nozzle cases and for $S_g = 1.45$ in particular, radical intensity is still strong near the nozzle even at $\Phi = 1.2$. Assuming some combination of OH*, NH* and NH_2* intensity can be used to represent heat release rate [29–32], the short nozzle cases having this centre of intensity farther away from the nozzle may reduce thermal degradation of the nozzle material over extended periods of use.

A difference in radical distribution and density between the swirlers can be seen in Fig. 4. All cases had a relatively compact distribution of OH*, NH* and NH_2* radicals at $\Phi = 0.8$. The two swirlers with short nozzles however had broadly distributed radicals with low density at $\Phi = 1.0$ and 1.2. The $S_g = 1.45$ long nozzle case was the only case to maintain a high radical density with a clearly defined flame front at $\Phi = 1.2$. These variations in distribution and density of key radicals with different swirl number and nozzle design may provide potential for controlling emissions.

Fig. 5 below shows the static stability map for each of the swirlers at a range of thermal powers. Lean blowoff (LBO) was found to be relatively independent of swirl number and nozzle geometry, with all cases having a similar LBO limit of around $\Phi = 0.4$ at 5 kW and 10 kW thermal power. Lean blowoff limits could not be reached here for 15 kW thermal power as the maximum flowrate of the air was 500 SLPM, representing roughly $\Phi = 0.5$ – at which all cases still had a stable flame. This is not an unprecedented finding, with Zhang et al. [33] previously reporting changes in swirl number having no apparent effect on extending LBO limits of pure NH_3 flames. One potential explanation for this relates to Lewis number and consumption rates. Su et al. [22] found that in an 18 % cracked NH_3 blend (with Lewis number <1), consumption rates of NH_3 and H_2 in the shear layer region increased as LBO was approached. This locally increased flame temperature, strengthening combustion near LBO. The opposite was found for fuels with Lewis number greater than unity, such as propane.

The $S_g = 1.45$ long nozzle case had the highest rich blowoff limits (RBO) at 5 kW, likely related to its jet-like behaviour, which meant it did not have to rely on the establishment of strong recirculation zones for stability. However, as thermal power – and hence dump plane velocity – increased, the RBO limit for the $S_g = 1.45$ long nozzle case reduced as low as $\Phi = 1.46$. This was due to an observed pinch-off phenomenon, where the flame separated into two parts – the long, jet like base and a more open cone shape at the head. This cone became detached from the base of the flame due to the high axial velocity at elevated thermal powers, eventually causing RBO. The beginnings of this effect can be seen at rich conditions in Figs. 3 and 4. This phenomenon was also observed for the $S_g = 1.75$ long nozzle case, but not to as extreme a degree. Conversely, as thermal power and dump plane velocity increased, the two short nozzle cases were able to form strong recirculation zones – not present at rich 5 kW conditions – widening rich stability limits significantly. It is posited that the short CRZ from the long nozzle causes high local curvature and stretch just downstream of the CRZ as the flow meets the central axis. As equivalence ratio increases, this highly strained region experiences local extinction, which causes the downstream flow to detach, resulting in blow-off. This pinch-off phenomenon has been previously observed by Zhang et al. [33] in pure NH_3 and 50/50 NH_3/H_2 flames, who suggested it was due to excessive stretch causing local extinction and a reduction in heat release rate.

To test the idea of the short nozzle enabling the flame to become wider with more resistance to necking and hence better performance at higher thermal powers, the swirl burner was placed into a larger combustor, as discussed in Section 2.1. Here, the same $S_g = 1.45$ long and short nozzles were tested at 100 kW and stoichiometric conditions. No modifications were made to the swirlers, nozzles nor burner architecture, the only difference was the size of the confinement downstream of the dump plane.

Fig. 6 shows there were significant differences in flame morphology. As in Figs. 3 and 4, the $S_g = 1.45$ long nozzle case presented as a near jet-like flame, anchored on the bluff body and with little in terms of external recirculation zones (ERZ) visible. The 100 kW condition shown here was the upper limit of stable flame achievable for the $S_g = 1.45$ long nozzle case. Additionally, the blowoff mechanism of "necking" or "pinch off" is

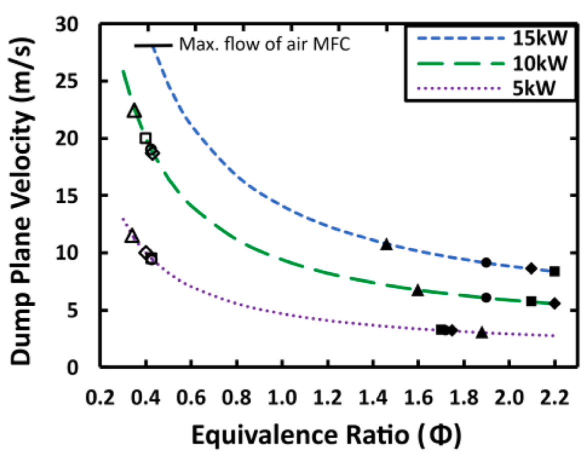

Fig. 5. Static stability map representing LBO and RBO for each of the swirlers at three thermal powers. Empty and filled symbols represent LBO and RBO, respectively. Squares for $S_g = 1.0$ short nozzle, diamonds for $S_g = 1.45$ short nozzle, triangles for $S_g = 1.45$ long nozzle, circles for $S_g = 1.75$ long nozzle.

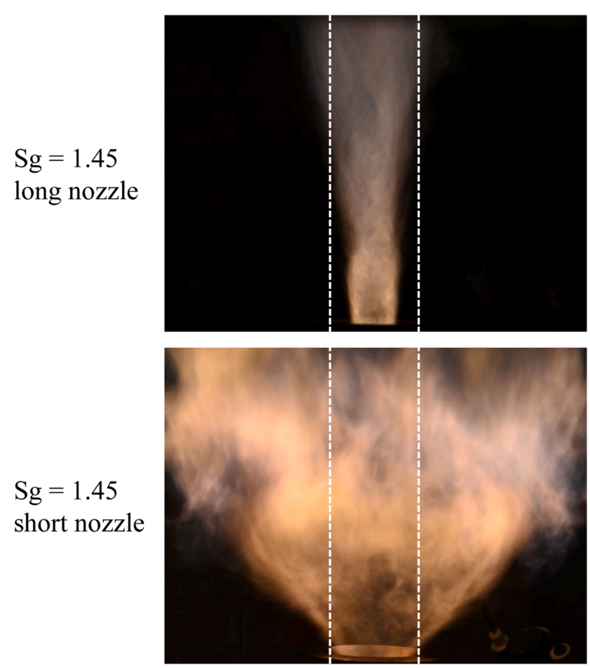

Fig. 6. Flame images of the $S_g = 1.45$ swirler with the long (top) and short (bottom) nozzles at a thermal power of 100 kW and $\Phi = 1.0$. Aperture = $F/4$, Exposure time = 1/400 s and ISO = 4000. Each image represents an area of 200 × 150 mm. White lines denote the diameter of the nozzle outlet, which was 1.4D for both nozzles.

clear to see in this photo. In comparison, the short nozzle case had a much lower flame angle, and a more classic V-shape flame anchored on the nozzle outlet. This difference in anchoring position is highlighted by the white lines superimposed on to both images, which demarcates the edge of the nozzle outlet, which was the same on both nozzles at 1.4D The short nozzle case also exhibits higher flame intensity, suggesting higher combustion efficiency.

3.2. Exhaust gas emissions

Having identified the potential for the short nozzle cases to improve static flame stability at elevated powers, the emissions performance was then examined.

Fig. 7 shows the emissions of NO, NO_2, NH_3 and N_2O for the four swirlers at 10 kW thermal power. The first noticeable result is at $\Phi = 0.6$ where flame instabilities caused a simultaneous and trend defying increase in NO and NH_3 emissions for three out of the four swirl cases, with the $S_g = 1.75$ long nozzle case being seemingly unaffected. The increase in NO here is posited to be related to small flame instabilities approaching lean blowoff which may cause local extinction. This could result in regions with slightly elevated – but still lean – local equivalence ratios, resulting in higher NO production. The $S_g = 1.75$ long nozzle case being unaffected is likely related to the significant difference in flame morphology shown in Fig. 3, where $S_g = 1.75$ long nozzle had a short, flat flame. Although this appears to present a desirable emissions profile with low NO and low unburned NH_3, the N_2O emissions here for $S_g = 1.75$ long nozzle – although relatively low compared to the other three swirlers – was still prohibitively high at around 450 ppm.

For $\Phi > 0.7$ in Fig. 7, overall emissions trends were more consistent. At $\Phi = 0.7$, NO and N_2O emissions appear linked, with reverse trends in terms of best emissions performance. For NO, $S_g = 1.45$ long had the lowest emissions, followed by $S_g = 1.0$ short, $S_g = 1.45$ short and then $S_g = 1.75$ long. This is the same order for descending flame length, as seen in Fig 8, suggesting this is related to flame length and hence residence

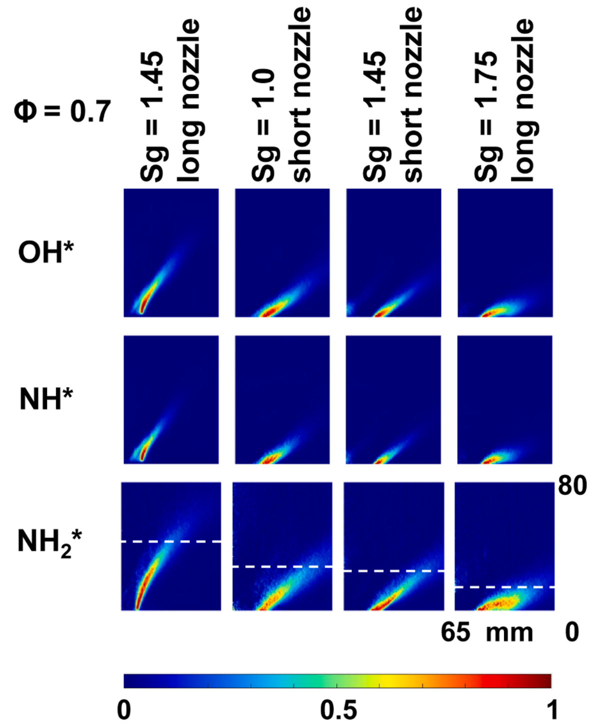

Fig. 8. Right half of Abel transformed chemiluminescence images (OH*, NH* and NH_2*) for each of the four cases at $\Phi = 0.7$ and 10 kW. Colourmap of images normalised to each image's maximum intensity. White dashed lines on NH_2* images denote flame height.

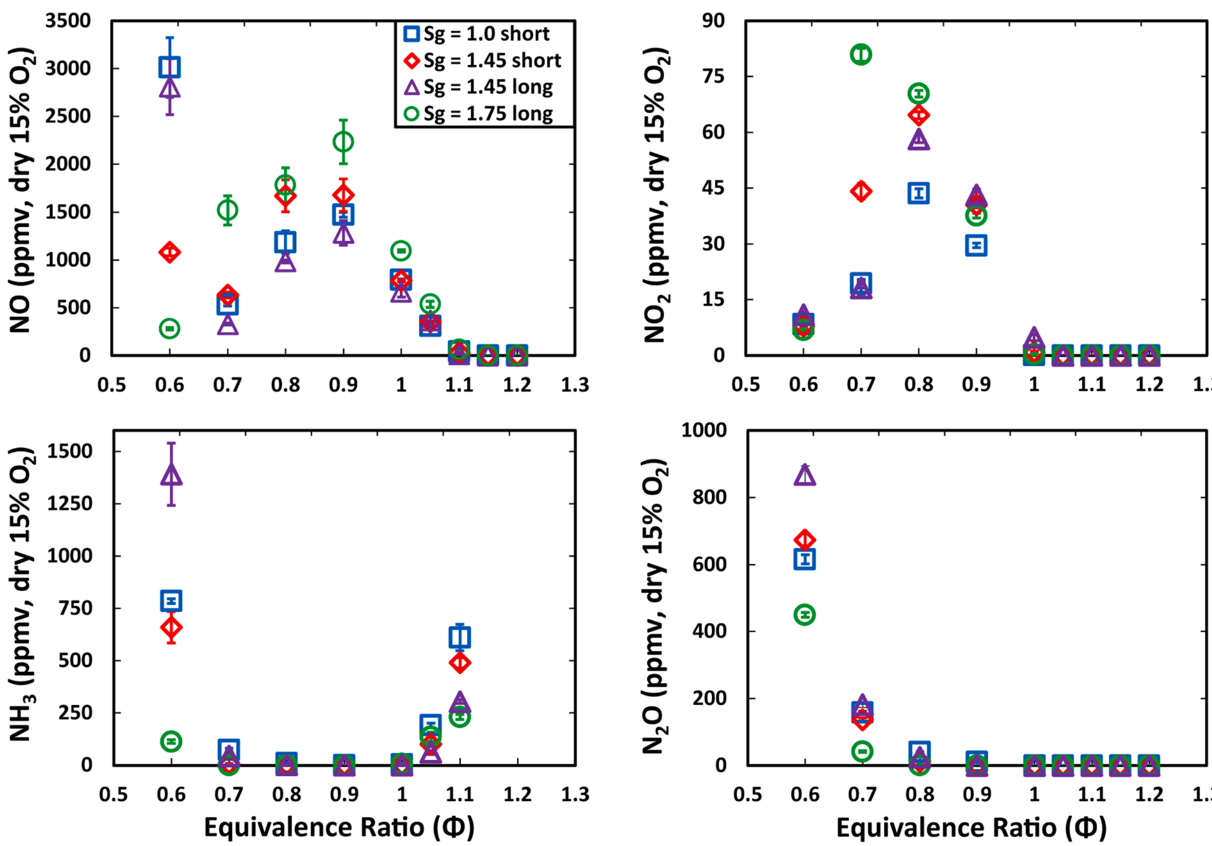

Fig. 7. Sampled emissions with changing equivalence ratio at 10 kW thermal power for the four swirler cases. Out of range NH_3 above $\Phi = 1.1$ not plotted.

time. The exact opposite order can be seen for N_2O. NO production is related to N_2O production via the reaction shown in Eq. (2) [34]. Fig. 8 shows that for the $S_g = 1.75$ long nozzle case at $\Phi = 0.7$, NH* and OH* intensity is concentrated near to the nozzle, with a nearly flat flame. This suggests that the NO formed from OH and NH via the HNO pathway described in Eqs. (3) and (4) [34] will be formed near the nozzle. Then, for the $S_g = 1.75$ long nozzle case, as there is little NH concentration axially downstream of the nozzle, there is little residence time for the NO to be converted into N_2O by NH. This would account for the high NO and low N_2O emissions profile shown for the $S_g = 1.75$ long nozzle case and the reverse shown for the $S_g = 1.45$ long nozzle case at $\Phi = 0.7$ in Fig. 7. Additionally, a study from Rieth et al. [35] found that high positive curvature in very lean partially cracked ammonia flames caused an increase in consumption of N_2O by the reaction show in Eq. (5) due to fast diffusion of hydrogen. Figs. 3 and 8 show high rates of positive curvature in the region near the nozzle for the $S_g = 1.75$ swirler at $\Phi = 0.6$ and 0.7, which may also contribute to the low N_2O emissions found here in Fig. 7. They also found that positive curvature can decrease NO emissions at very lean conditions of $\Phi = 0.45$, while the opposite is true at $\Phi = 0.9$. Although the authors did not suggest an exact crossover equivalence ratio for this effect, it may explain why NO emissions remained comparatively low at $\Phi = 0.6$ but comparatively high at $\Phi = 0.7$ for the $S_g = 1.75$ case in Fig. 7. The findings of increased NO at positively curved regions from [36] due to preferential diffusion of H_2 also support this increase at $\Phi = 0.7$ for the $S_g = 1.75$ case.

$$NH + NO \leftrightarrow N_2O + H \tag{2}$$

$$NH + OH \leftrightarrow HNO + H \tag{3}$$

$$HNO + H \leftrightarrow NO + H_2 \tag{4}$$

$$N_2O + H \leftrightarrow OH + N_2 \tag{5}$$

Temperatures measured by an R-type thermocouple situated 50 mm upstream of the combustor exit is shown in Fig. 9. Discounting the flat flame phenomenon found for the $S_g = 1.75$ long nozzle case at $\Phi < 0.8$, a very clear trend can be seen. Due to the fixed location of the thermocouple, measured temperatures in the post-flame zone were a function of flame length, with the exhaust from shorter flames having a longer time for heat loss to the confinement wall to reduce temperatures. At $\Phi = 0.7$, measured temperatures also correlated with the order of flame length for each of the cases, as shown in Fig. 8.

Discounting outliers due to flame instabilities at $\Phi = 0.6$, NO emissions peaked for all cases at $\Phi = 0.9$ and reached negligible values at $\Phi = 1.15$. In this study, emissions were considered negligible when the gas analyser measured 0.0 ppmv. The lowest emissions of NO were found with the $S_g = 1.45$ long nozzle case. There are clear trends with the Sg = 1.0 short nozzle case offering the next best NO performance, followed by the other short nozzle case and then the Sg = 1.75 long nozzle case. This shows that NO emissions are dependent on both swirl number and nozzle geometry, with good performance achievable with low swirl and a short nozzle, as well as medium swirl and a long nozzle. For the $S_g = 1.45$ case, NO emissions were generally lower with a longer nozzle. This could potentially also relate to flame length, with the longer nozzle producing a longer flame with enhanced residence time for the consumption of NO by NH_2. Emissions of unburned NH_3 followed the opposite trend, measured at sub 5ppmv for $0.7 < \Phi \leq 1.0$ and rapidly increasing at rich conditions for all swirlers. Negligible emissions of N_2O were recorded for $\Phi > 0.9$ due to flame temperatures and residence times increasing sufficiently to consume N_2O fully. If N_2O emissions were solely temperature dependent, it could be expected for them to increase again at rich conditions, as Fig. 9 shows similarly low temperatures for $\Phi > 1.1$ and $\Phi < 0.8$. However, the long flames shown in Fig. 3 at rich conditions facilitate the conversion of N_2O back into NO, despite lower temperatures. Emissions of NO_2 followed similar trends to NO and reached negligible values at $\Phi = 1.05$ so are therefore not discussed in detail in the present paper.

As the lean conditions plotted in Fig. 7 do not present simultaneously low NO, N_2O and NH_3 emissions, attention is turned to slightly rich conditions instead. Fig. 10 below shows the emissions of NO and NH_3 for the four swirlers. For $\Phi \leq 1.05$, these emissions comprise mainly of NO, and at $\Phi = 1.1$, the emissions are mainly unburned NH_3. The lower limit found for emissions at any equivalence ratio was with the $S_g = 1.45$ long nozzle case, reaching 318 ppm comprising 14 ppm NO and 304 ppm NH_3, with negligible NO_2 and N_2O emissions at $\Phi = 1.1$. This represents good potential for the primary stage of an air staged combustor, with a secondary air stage to burn the remnant NH_3. The $S_g = 1.45$ short nozzle case had 30 ppm NO emissions but 60 % higher NH_3 emissions. The reason for the significant increase in unburned NH_3 for the short nozzle case may be related to the confinement diameter. Due to the short nozzle causing the flames to open significantly more than the long nozzles, flame impingement on the quartz glass cylinder may be an issue, as suggested for the $\Phi = 1.2$ images in Fig. 4. Flame impingement on the confinement walls would increase heat loss, hence reducing combustion efficiency. This is confirmed in Fig 9, which shows the two short nozzles had the lowest measured post-flame zone temperatures. Due to these cases having equal flowrates and consequently equal adiabatic flame temperatures, the measured differences can only be due to differences in heat losses. It should be noted that the elevated NH_3 emissions measured with the short nozzles could be avoided by slightly increasing the diameter of the confinement. It is not expected to be an issue with the industrial system shown in Fig. 6 due to it having a confinement diameter nearly 5x larger than the lab-scale system shown in Fig. 1. The industrial system will also feature a scaled-up version of the burner presented in this study. Despite this, the future pairing possesses an expansion ratio from burner dump plane area to confinement area of 82.8, which is significantly higher than the expansion ratio of 50.1 in the lab-scale system. This should prevent any flame impingement on the

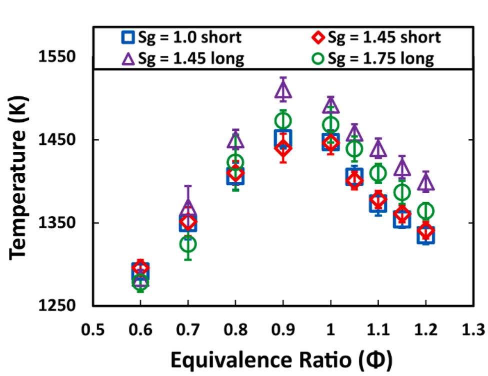

Fig. 9. Temperature measured in the post-flame zone 50 mm upstream of the combustor exit (corrected for radiative and convective heat loss from the thermocouple).

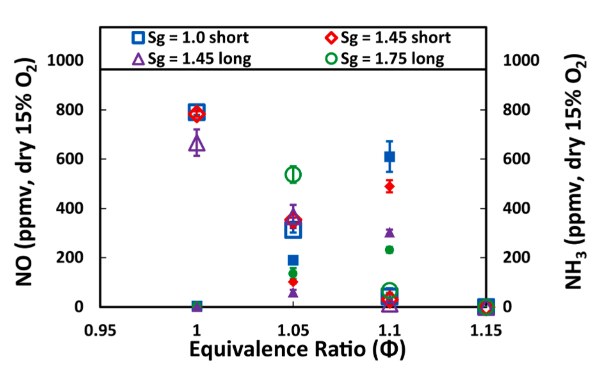

Fig. 10. Emissions of NO and NH_3 at slightly rich conditions and 10 kW thermal power for the four swirler cases. Out of range NH_3 above $\Phi = 1.1$ not plotted. Open and solid symbols represent NO and NH_3 respectively.

confinement walls and associated increase in NH_3 emissions.

4. Conclusions

In this study, the effect of varying swirl number and nozzle geometry was investigated for 20 % cracked ammonia flames at a wide range of equivalence ratios ($0.3 < \Phi < 2.2$) and thermal powers of 5, 10, 15 and 100 kW.

Stable flames were achieved across a broad range of equivalence ratios with varying thermal power, swirl number and nozzle geometry. Flame morphology was strongly influenced by both swirl number and nozzle length, Notably, the case with the highest swirl number and a long nozzle exhibited a flat, Coanda jet flow flame at the leanest conditions.

Swirl number and nozzle geometry were found to have little effect on lean blowoff limits, supporting previous studies in the literature which suggest flames with a Lewis number below unity increase fuel consumption and hence increase flame temperature and burning velocity when approaching lean blowoff.

Conversely, a shorter nozzle resulted in significantly higher rich blowoff limits by widening the flame brush to avoid jet-like flames which are prone to pinching off. It is suggested that a long nozzle restricts the flow downstream of the dump plane from expanding radially, hindering the formation of the ERZ and shortening the CRZ. The confinement of the nozzle may result in a highly strained region just downstream of the CRZ which experiences local extinction as equivalence ratio increases, causing the downstream section of the flame to detach, resulting in rich blowoff. A wide flame brush was demonstrated to be a desirable characteristic in preventing this process and thus achieving higher thermal power for a given nozzle throat diameter.

While the $S_g = 1.45$ long nozzle case offered the lowest NO emissions, NO emissions with the $Sg = 1.0$ short nozzle case were not significantly higher. This shows that various permutations of nozzle geometry and swirl number can achieve similar NO emissions. For a constant geometric swirl number of 1.45, the long nozzle generally had slightly lower emissions, potentially due to the longer nozzles providing longer flames with increased residence time for consumption of NO by NH_2. However, at rich conditions this difference was smaller, and both long and short nozzles reached negligible NO emissions by $\Phi = 1.15$. With a wider flame brush, it is important to avoid flame impingement upon confinement walls, which can lead to increased local heat loss and hence reduced combustion efficiency.

CRediT authorship contribution statement

Jordan Davies: Writing – original draft, Visualization, Methodology, Investigation, Formal analysis, Data curation. **Daisuke Sato:** Writing – review & editing, Investigation, Data curation. **Syed Mashruk:** Writing – review & editing, Supervision, Funding acquisition. **Agustin Valera-Medina:** Writing – review & editing, Supervision, Funding acquisition.

Declaration of competing interest

The authors declare that they have no known competing financial interests or personal relationships that could have appeared to influence the work reported in this paper.

Acknowledgements

This work was supported by the AMBURN project with funding from the Department for Energy Security and Net Zero (DESNZ) (Grant Number: IFS2–06-FLO) and the EPSRC Centre for Doctoral Training in Resilient Decarbonised Fuel Energy Systems (Grant Number: EP/S022996/1). The research was undertaken at Cardiff University's Thermofluids Lab (W/0.17) and Combustion Lab (W/0.03) with invaluable technical support from Mr Jonathan Martin. Information on the data underpinning this publication, including access details, can be found in the Cardiff University Research Data Repository at [https://doi.org/10.17035/cardiff.29107994].

Data availability

Data will be made available on request.

References

[1] Kobayashi H, Hayakawa A, Somarathne KDKA, Okafor EC. Science and technology of ammonia combustion. Proc Combust Inst 2019;37:109–33. https://doi.org/10.1016/J.PROCI.2018.09.029.
[2] Valera-Medina A, Amer-Hatem F, Azad AK, Dedoussi IC, De Joannon M, Fernandes RX, et al. Review on ammonia as a potential fuel: from synthesis to economics. Energy and Fuels 2021;35:6964–7029. https://doi.org/10.1021/ACS.ENERGYFUELS.0C03685/ASSET/IMAGES/MEDIUM/EF0C03685_0038.GIF.
[3] Elbaz AM, Wang S, Guiberti TF, Roberts WL. Review on the recent advances on ammonia combustion from the fundamentals to the applications. Fuel Communications 2022;10:100053. https://doi.org/10.1016/J.JFUECO.2022.100053.
[4] Mashruk S, Vigueras-Zuniga MO, Tejeda-del-Cueto ME, Xiao H, Yu C, Maas U, et al. Combustion features of CH4/NH3/H2 ternary blends. Int J Hydrogen Energy 2022;47:30315–27. https://doi.org/10.1016/J.IJHYDENE.2022.03.254.
[5] Shi X, Lian T, Zhang Y, Liu Z, Li W, Xi Z, et al. Enhanced ammonia combustion by partial pre-cracking strategy in a gas turbine model combustor: flame macrostructures, lean blowout characteristics and exhaust emissions. Applications in Energy and Combustion Science 2024;17:100247. https://doi.org/10.1016/J.JAECS.2024.100247.
[6] Monge-Palacios M, Zhang X, Morlanes N, Nakamura H, Pezzella G, Sarathy SM. Ammonia pyrolysis and oxidation chemistry. Prog Energy Combust Sci 2024;105:101177. https://doi.org/10.1016/J.PECS.2024.101177.
[7] Verkamp FJ, Hardin MC, Williams JR. Ammonia combustion properties and performance in gas-turbine burners. Symposium (International) on Combustion 1967;11:985–92. https://doi.org/10.1016/S0082-0784(67)80225-X.
[8] Valera-Medina A, Morris S, Runyon J, Pugh DG, Marsh R, Beasley P, et al. Ammonia, methane and hydrogen for gas turbines. Energy Procedia 2015;75:118–23. https://doi.org/10.1016/J.EGYPRO.2015.07.205.
[9] Kurata O, Iki N, Matsunuma T, Inoue T, Tsujimura T, Furutani H, et al. Performances and emission characteristics of NH3–air and NH3CH4–air combustion gas-turbine power generations. Proc Combust Inst 2017;36:3351–9. https://doi.org/10.1016/J.PROCI.2016.07.088.
[10] Okafor EC, Somarathne KDKA, Hayakawa A, Kudo T, Kurata O, Iki N, et al. Towards the development of an efficient low-NOx ammonia combustor for a micro gas turbine. Proc Combust Inst 2019;37:4597–606. https://doi.org/10.1016/J.PROCI.2018.07.083.
[11] Hayakawa A, Arakawa Y, Mimoto R, Somarathne KDKA, Kudo T, Kobayashi H. Experimental investigation of stabilization and emission characteristics of ammonia/air premixed flames in a swirl combustor. Int J Hydrogen Energy 2017;42:14010–8. https://doi.org/10.1016/J.IJHYDENE.2017.01.046.
[12] Valera-Medina A, Gutesa M, Xiao H, Pugh D, Giles A, Goktepe B, et al. Premixed ammonia/hydrogen swirl combustion under rich fuel conditions for gas turbines operation. Int J Hydrogen Energy 2019;44:8615–26. https://doi.org/10.1016/J.IJHYDENE.2019.02.041.
[13] Pugh D, Bowen P, Valera-Medina A, Giles A, Runyon J, Marsh R. Influence of steam addition and elevated ambient conditions on NOx reduction in a staged premixed swirling NH3/H2 flame. Proc Combust Inst 2019;37:5401–9. https://doi.org/10.1016/J.PROCI.2018.07.091.
[14] Khateeb AA, Guiberti TF, Zhu X, Younes M, Jamal A, Roberts WL. Stability limits and NO emissions of technically-premixed ammonia-hydrogen-nitrogen-air swirl flames. Int J Hydrogen Energy 2020;45:22008–18. https://doi.org/10.1016/J.IJHYDENE.2020.05.236.
[15] Khateeb AA, Guiberti TF, Wang G, Boyette WR, Younes M, Jamal A, et al. Stability limits and NO emissions of premixed swirl ammonia-air flames enriched with hydrogen or methane at elevated pressures. Int J Hydrogen Energy 2021;46:11969–81. https://doi.org/10.1016/J.IJHYDENE.2021.01.036.
[16] Wang G, Guiberti T, Roberts W. Exploring the effects of swirl intensity on NO emission in Ammonia-methane-air premixed swirling flames. Journal of Ammonia Energy 2023;1. https://doi.org/10.18573/JAE.14.
[17] Chen D, Li J, Li X, Guo Y, Huang H, Kobayashi N. Experimental studies on the OH* chemiluminescence and structure characteristics in NH3/H2 and NH3/cracked gas swirl flames. Int J Hydrogen Energy 2024;52:1370–9. https://doi.org/10.1016/J.IJHYDENE.2023.06.185.
[18] Sato D, Davies J, Mazzotta L, Mashruk S, Valera-Medina A, Kurose R. Effects of reynolds number and ammonia fraction on combustion characteristics of premixed ammonia-hydrogen-air swirling flames. Proc Combust Inst 2024;40. https://doi.org/10.1016/j.proci.2024.105283.
[19] Mashruk S, Zitouni SE, Brequigny P, Mounaim-Rousselle C, Valera-Medina A. Combustion performances of premixed ammonia/hydrogen/air laminar and

swirling flames for a wide range of equivalence ratios. Int J Hydrogen Energy 2022;47:41170–82. https://doi.org/10.1016/J.IJHYDENE.2022.09.165.
[20] Zitouni S, Bréquigny P, Mounaïm-Rousselle C. Turbulent partially cracked ammonia/air premixed spherical flames. Fuel Communications 2024;20:100126. https://doi.org/10.1016/J.JFUECO.2024.100126.
[21] Su T, Xu B, Bastiaans RJM, Worth NA. Lean blow-off behaviour of premixed bluff-body stabilized hydrocarbon-air flames and ammonia/hydrogen/nitrogen-air flames. J Eng Gas Turbine Power 2024;146. https://doi.org/10.1115/1.4065908/1201481.
[22] Su T, Xu B, Bastiaans RJM, Worth NA. The behaviour of NH3/H2/N2, CH4 and C3H8 turbulent premixed bluff-body stabilized flames near lean blow-off. Proc Combust Inst 2024;40:105739. https://doi.org/10.1016/J.PROCI.2024.105739.
[23] Claypole T.C., Syred N. The effect of swirl burner aerodynamics on NOx formation 1981.
[24] Dasch CJ. One-dimensional tomography: a comparison of Abel, onion-peeling, and filtered backprojection methods. Appl Opt 1992;31:1146–52.
[25] British Standards Institute. British Standard ISO 11042-1:1996, gas turbines. Exhaust gas emission measurement and evaluation. 1996.
[26] Vanierschot M, Van den Bulck E. Hysteresis in flow patterns in annular swirling jets. Exp Therm Fluid Sci 2007;31:513–24. https://doi.org/10.1016/J.EXPTHERMFLUSCI.2006.06.001.
[27] Holemans T, Yang Z, De Greef J, Vanierschot M. Swirl-induced hysteresis in a sudden expansion flow. Physics of Fluids 2024;36:105193. https://doi.org/10.1063/5.0231799/3318267.
[28] Singh NK, Ramamurthi K. Formation of Coanda jet from sharp-edged swirl nozzle with base plate. Exp Therm Fluid Sci 2009;33:675–82. https://doi.org/10.1016/J.EXPTHERMFLUSCI.2009.01.008.
[29] Mashruk S, Xiao H, Pugh D, Chiong MC, Runyon J, Goktepe B, et al. Numerical analysis on the evolution of NH2 in Ammonia/hydrogen swirling flames and detailed sensitivity analysis under elevated conditions. Combustion Science and Technology 2023;195:1251–78. https://doi.org/10.1080/00102202.2021.1990897.
[30] Cosway B, Talibi M, Balachandran R. Investigation of NO production and flame structures in ammonia-hydrogen flames. Journal of Ammonia Energy 2023:106–17. https://doi.org/10.18573/jae.20.
[31] Xing J, Pillai AL, Kurose R. Heat release rate surrogate for ammonia–hydrogen premixed flames under various conditions. Applications in Energy and Combustion Science 2023;15:100193. https://doi.org/10.1016/J.JAECS.2023.100193.
[32] Wei Y, Zhu X, Tian B, Zhou H, Issayev G, Cheng YB, et al. Excited species as heat release rate markers in Laminar premixed Ammonia-hydrogen-air flames. Energy and Fuels 2024;38:11311–20. https://doi.org/10.1021/ACS.ENERGYFUELS.4C01501/ASSET/IMAGES/LARGE/EF4C01501_0012.JPEG.
[33] Zhang M, Wei X, Wang J, Huang Z, Tan H. The blow-off and transient characteristics of co-firing ammonia/methane fuels in a swirl combustor. Proc Combust Inst 2021;38:5181–90. https://doi.org/10.1016/J.PROCI.2020.08.056.
[34] Mashruk S, Okafor EC, Kovaleva M, Alnasif A, Pugh D, Hayakawa A, et al. Evolution of N2O production at lean combustion condition in NH3/H2/air premixed swirling flames. Combust Flame 2022;244:112299. https://doi.org/10.1016/J.COMBUSTFLAME.2022.112299.
[35] Rieth M, Gruber A, Chen JH. A direct numerical simulation study on NO and N2O formation in turbulent premixed ammonia/hydrogen/nitrogen-air flames. Proc Combust Inst 2023;39:2279–88. https://doi.org/10.1016/J.PROCI.2022.07.266.
[36] Chi C, Han W, Thévenin D. Effects of molecular diffusion modeling on turbulent premixed NH3/H2/air flames. Proc Combust Inst 2023;39:2259–68. https://doi.org/10.1016/J.PROCI.2022.08.074.